Entanglement in a holographic Schwinger pair with confinement

Sebastian Grieninger,[1,*] Dmitri E. Kharzeev,[1,2,†] and Ismail Zahed[1,‡]

[1]*Center for Nuclear Theory, Department of Physics and Astronomy, Stony Brook University, Stony Brook, New York 11794–3800, USA*

[2]*Department of Physics, Brookhaven National Laboratory, Upton, New York 11973-5000, USA*

(Received 28 June 2023; accepted 5 October 2023; published 26 October 2023)

We revisit the entanglement of a Schwinger pair created by external fields of arbitrary strength, using a holographic dual description of QCD. When external fields are strong in comparison to the string tension, the entanglement is geometrically tied to the Einstein-Rosen (ER) bridge in the bulk, and disappears when the pair production is not exponentially suppressed at the boundary. For moderate external fields, the entanglement is shown to follow from the geometrical interplay between the position of the ER bridge and the confining wall in the bulk. We clarify the physical nature of quantum entanglement in pair production, and connect it to the entropy of entanglement between the left- and right-moving fermions. In particular, we clarify the effect of real radiation off the produced particles on quantum entanglement of the pair.

DOI: 10.1103/PhysRevD.108.086030

I. INTRODUCTION

Entanglement underlies the quantum description of physical laws. Quantum states are complex superposition states in a Hilbert space, with a content that is revealed by the projection measurement. As a result, two noncausally related measurements can be correlated.

A striking example of these noncausal correlations is the famous Einstein-Rosen-Podolsky (EPR) paradox. The common realization of this paradox is that of an entangled pair of spin-$\frac{1}{2}$ in an initial spin singlet state, with spins that are correlated at spacelike separations. In particular, this canonical setup allows to derive the simplest Bell inequality that rules out the concept of hidden variables in quantum mechanics.

Recently, the quantum entanglement in Schwinger pair creation process [1] was described using a gravity dual description [2,3]. Remarkably, the dual of the EPR pair in bulk is a string [4–11] with a world sheet that sustains a nontraversable wormhole [Einstein-Rosen (ER) bridge], suggesting the equivalence between the entanglement and the wormholes within the holographic correspondence [12]. The extension to traversable wormholes was further worked out in [13]. The possible applications entanglement in pair production to phenomenology of high energy hadron and nuclear collisions were discussed in [14,15].

In the Schwinger quark-antiquark pair production, the endpoints are never causally connected. Nevertheless, the pair is entangled due to its overall color neutrality. In nonconfining dual gravity description, the entanglement was found to be of order $\sqrt{\lambda}$ in the weak field limit [2,9], where $\lambda = g_Y^2 N_c$ is the 't Hooft strong coupling.

Outside of the holographic framework, the entanglement in Schwinger pair production was addressed in [16], without considering the radiation emitted by the produced particles. It has been found there that the entropy of entanglement between the left-moving antifermions and the right-moving fermions is exactly equal to the statistical Gibbs entropy of the produced state. It is of great interest to check whether this intriguing relation is modified in the presence of radiation off the produced fermions. Recent quantum simulations indicate that radiation off the produced pair reduces the amount of entanglement [17].

In this work, we will extend the holographic treatment of Schwinger pair production to the external U(1) fields of arbitrary strength, and consider also the effects of confinement. The first study of the holographic Schwinger process in a confining background was carried out in [18], where a critical threshold for the electric field was noted. The case of pair production in a confining geometry was studied also in [19], and it was found that the wormhole does not appear when the quark and antiquark are separated in the transverse space. The emergence of horizon, and the ensuing interpretation of Schwinger pair production in terms of thermal Hawking-Unruh radiation was discussed in [14,20].

The organization of the paper is as follows: In Sec. II we briefly outline the effect of confinement on the Schwinger

*sebastian.grieninger@stonybrook.edu
†dmitri.kharzeev@stonybrook.edu
‡ismail.zahed@stonybrook.edu

pair creation process. Confinement inhibits the pair production, unless the applied electric field is sufficiently strong to overcome the effect of the confining string. In Sec. III we discuss the holographic setup in the weak field limit for Schwinger pair production. Mikhailov's light-like surface [21] for a quark and antiquark receding at a constant lightlike acceleration in conformal AdS_5 is used to evaluate the bulk action explicitly. The emerging Unruh temperature allows for the extraction of the free energy. We identify the quantum entanglement entropy with the ensuing thermal entropy. The results are readily extended to "walled" AdS_5 to account for confinement. In Sec. IV we extend the holographic setup to the strong field limit, and derive the quantum entanglement entropy for the conformal and confining geometries in curved AdS. In Sec. V we make a link to phenomenology by using a schematic form of the Lund model to derive the entanglement entropy associated to the string fragmentation in jets. This entanglement entropy measures the Schwinger pair creation probability. This entropy is smaller than the single tunneling entanglement entropy from the confining geometry, owing to the decoherence due to the random tunnelings, yet it should be accessible to experimental measurements. Our conclusions are in Sec. VI.

II. PAIR CREATION

Before we detail the holographic analysis of the Schwinger pair creation process in a confining AdS background, let us discuss the general features of this process. It is clear that to produce a pair of quarks with mass M from the vacuum, an electric field E should lose energy in excess of $2M$. In the presence of confinement described by a linear quark-antiquark potential $\sigma_T r$ (where σ_T is the string tension), this requirement is made more prohibitive with the threshold set at $2M + \sigma_T r$, with r the pair separation. With this in mind, the effective potential for a $q\bar{q}$ pair undergoing pair production is typically of the form

$$V_{\rm eff}(r) = 2M - (E - \sigma_T) r - \frac{C\sqrt{\lambda}}{r}, \tag{1}$$

where we have added the attractive Coulomb-type quark-antiquark interaction that is important at short distances; $\lambda = g_Y^2 N_c$ is the strong 't Hooft coupling, and the constant C was fixed in [22]. Throughout this paper, we include the coupling g_Y in the definition of E.

The potential (1) is illustrated in Fig. 1. Clearly, for $E < \sigma_T$, the confined pair cannot be separated and pair production is prohibited. Pair production is only possible if $E > \sigma_T$, for which the tunneling through the potential barrier is exponentially suppressed. For sufficiently strong fields, $E > E_c > \sigma_T$, the barrier vanishes, and pair production is no longer penalized. Without confinement (when $\sigma_T = 0$), a simple estimate of E_c can be made by assuming that the work done by electric field $E_c r$ should match $2M$ at

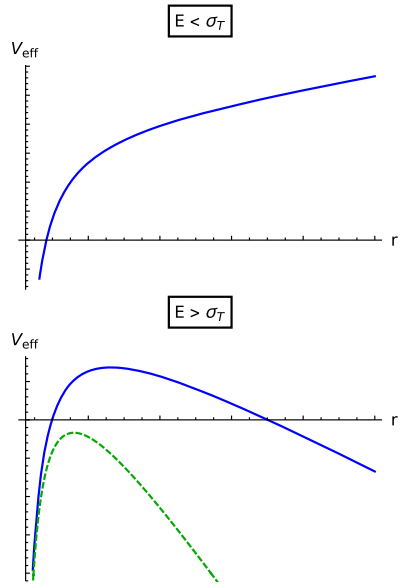

FIG. 1. Effective potential $V_{\rm eff}(r)$ versus the distance, for weak (top) and strong (bottom) electric field ($E_c > E > \sigma_T$: blue, $E > E_c > \sigma_T$: green, dashed).

distance where the energy of the strong Coulomb attraction equals $2M$,

$$E_c r \sim 2M \sim \frac{C\sqrt{\lambda}}{r}. \tag{2}$$

This relation yields $r \sim C\sqrt{\lambda}/2M$, and

$$E_c \sim \frac{4M^2}{C\sqrt{\lambda}}. \tag{3}$$

With confinement, the critical value is shifted by the string tension, $E_c \to E_c + \sigma_T$.

III. HOLOGRAPHIC SETUP: WEAK FIELD

To address the pair production in a holographic setup modeling QCD, we will use a bottom-up approach. In the double limit of large N_c (at fixed number of flavors N_f) and strong 't Hooft coupling λ, quarks are permanently confined with no string breaking. Large Wilson loops exhibit an area law at all distances. In the gravity dual, the area law follows from a simple AdS_5 with a hard wall [23], with a line element

$$ds^2 = \frac{L^2}{z^2}((dx^\mu)^2 + dz^2) \qquad z \le z_H. \tag{4}$$

and zero otherwise. The string tension is readily found to be

$$\sigma_T = \frac{1}{2\pi\alpha'}\frac{L^2}{z_H^2} = \frac{\sqrt{\lambda}}{2\pi}\frac{1}{z_H^2}. \tag{5}$$

Here α' is the Regge slope for an open string, fixed by the ρ meson trajectory $\alpha' = 1/2m_\rho^2$. Inside the QCD string, the strength of the chromoelectric field is proportional to the string tension $E \simeq 4\sigma_T$ [24].

For $z_H \to \infty$ at fixed coupling, the string tension vanishes and (4) reduces to conformal AdS_5. We will start our discussion with this latter case to clarify some issues regarding the evaluation of the entanglement entropy, and then proceed to the pair creation process in the confining case.

A. AdS_5

The holographic Schwinger effect in conformal AdS was discussed in [5,11], using a string world sheet in Euclidean signature. In Minkowski signature, the world sheet is the ruled surface of delayed rays in the bulk [4,10,21,25],

$$X^M(\tau, z) = (z\dot{x}^\mu(\tau) + x^\mu(\tau), z) \tag{6}$$

with the 4d hyperbolic trajectories on the boundary

$$x^\mu_\pm(\tau) = \left(\frac{1}{a}\sinh(a\tau), \pm\frac{1}{a}\cosh(a\tau), 0, 0\right) \tag{7}$$

for constant acceleration $a = E/M$. The world sheet (6) and (7) is a hyperboloid

$$X_M^2 = -t^2 + x^2 + z^2 = x_\mu^2(\tau) = \frac{1}{a^2} \tag{8}$$

as illustrated in Fig. 2 for $a^2 = \dot{x}^2 \equiv 1$. The line element associated to (6) is

$$\mathrm{d}X^M = (\mathrm{d}z\dot{x} + za\mathrm{d}\tau + \dot{x}\mathrm{d}\tau, \mathrm{d}z). \tag{9}$$

The determinant of the induced metric of the world sheet embedded in AdS_5 is given by

$$\det\left(g_{mn}\frac{\partial X^m}{\partial\nu}\frac{\partial X^n}{\partial\sigma}\right) = \det\begin{pmatrix} \frac{L^2}{z^2}(za+\dot{x})^2 & \frac{L^2}{z^2}\dot{x}(za+\dot{x}) \\ \frac{L^2}{z^2}\dot{x}(za+\dot{x}) & \frac{L^2}{z^2}(\dot{x}^2+1)\end{pmatrix}$$
$$= \det\begin{pmatrix} L^2(a^2 - \frac{1}{z^2}) & -\frac{L^2}{z^2} \\ -\frac{L^2}{z^2} & 0\end{pmatrix}, \tag{10}$$

since $\dot{x}^2 = -1$ and $0 = \mathrm{d}/\mathrm{d}\tau(\dot{x}^2) = 2a\dot{x}$.

Remarkably, (6) can be regarded as the locus of the radiated gluons between the receding pairs at strong coupling, as captured by dual gravity, with the power radiated at the boundary [4,21]

$$\frac{d\mathcal{E}}{dt} = \frac{\sqrt{\lambda}}{2\pi}a^2 \tag{11}$$

This is to be compared to the weak coupling, classical dipole-like Larmor emission with the total radiated power P

$$P = \frac{2}{3}g_Y^2 a^2 \tag{12}$$

Causal contribution:

From (10) we note the appearance of a horizon at $z = \frac{1}{a}$, whereby the produced pair loses causal contact [2,4]. With this in mind, the Nambu-Goto action supported by the causal part of the world sheet is

$$\Delta S = 2 \times \frac{1}{2\pi\alpha'}\int_{-\mathcal{T}/2}^{\mathcal{T}/2}\mathrm{d}\tau\int_{z_M}^{1/a}\mathrm{d}z\frac{\alpha'\sqrt{\lambda}}{z^2}$$
$$= \frac{\sqrt{\lambda}}{2\pi}\mathcal{T}2\left(\frac{1}{z_M} - a\right) = 2\mathcal{T}\left(M - \frac{a\sqrt{\lambda}}{2\pi}\right), \tag{13}$$

after using (10). The overall factor of 2 counts the two separate sheet contributions in Fig. 2, when cut at $\frac{1}{a}$. The contribution from the boundary interaction term using (7), is

$$\Delta S_B = -2 \times \frac{E}{2}\int_{-\mathcal{T}/2}^{\mathcal{T}/2} d\tau(\dot{x}^0_+(\tau)x^1_+(\tau) - x^0_+(\tau)\dot{x}^1_+(\tau))$$
$$= -M\mathcal{T} \tag{14}$$

Combining (13) with (14) yields the energy *per particle*,

$$\frac{\mathcal{E}}{2} = \left(M - \sqrt{\lambda}T_U - \frac{M}{2}\right), \tag{15}$$

with the Unruh temperature $T_U = a/(2\pi)$. The temperature correction is reminiscent of the Debye correction to charge particle's self-energy

$$\mathcal{E}_D \sim -\lambda\frac{e^{-m_D r}}{r} \sim -\lambda m_D \sim -\lambda^{\frac{3}{2}}T_U, \tag{16}$$

at weak coupling, where we used $r \sim {m_D}^{-1}$, $m_D \sim \sqrt{\lambda}T_U$ for an estimate. The entanglement entropy follows

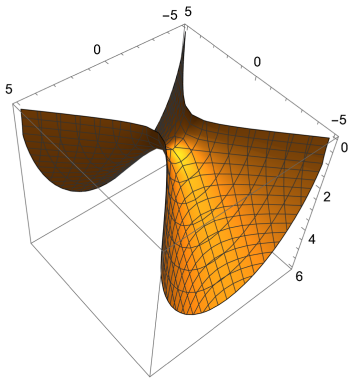

FIG. 2. Hyperboloid world sheet $-t^2 + x^2 + z^2 = \frac{1}{a^2} \equiv 1$ for $|x|, |t| \le 5$ and $0 \le z \le 6$.

from (15) if we interpret it as a free energy F of the particle at the Unruh temperature [9,11], and use the thermodynamic relation

$$S_{\rm EE} = -\frac{\partial \mathcal{E}/2}{\partial T_U} = \sqrt{\lambda}. \tag{17}$$

Noncausal contribution:

The remainder of the action comes from the noncausal contribution and describes the radiation from the produced pair. We will now see that this radiation reduces the amount of entanglement.

Let us begin by noting that the induced metric on the world sheet

$$\mathrm{d}X_M^2 = L^2\left(a^2 - \frac{1}{z^2}\right)\mathrm{d}\tau^2 - \frac{2L^2}{z^2}\mathrm{d}\tau\,\mathrm{d}z. \tag{18}$$

may be written as the metric of a topological black hole [26,27]. This is manifest, if we set $w = 1/(az)$ and $\tau = t/a - 1/a\,\mathrm{arctanh}\,w$ [28], so that (18) reads

$$\mathrm{d}X_M^2 = -(w^2-1)\mathrm{d}t^2 + \frac{\mathrm{d}w^2}{w^2-1}, \tag{19}$$

which clearly exhibits a world-sheet horizon for $w_h = 1$ (corresponding to $z = 1/a$).

1. Hyperbolic black hole

The induced metric in (19) can be regarded as a hyperbolic black hole metric in $\mathrm{d}+1$-dimensions, with a warping factor [6]

$$h(w) = w^2 - 1 - \frac{\mu}{w^{d-2}} \tag{20}$$

in the limit $\mu \to 0$. The horizon is fixed by the condition $h(w_h) = 0$, or

$$\mu = w_h^{d-2}(w_h^2 - 1) \tag{21}$$

with an inverse Rindler temperature

$$\beta_h = \frac{4\pi}{h'(w_h)} \overset{\mu\to 0}{\to} 2\pi \tag{22}$$

or the Unruh temperature $T_U = a/\beta_h$ as $\mu \to 0$. This result is based on the observation that hyperbolic coordinates in AdS correspond to a Rindler state of the CFT in Minkowski space at temperature $\beta_h = 2\pi/w_h$ [26,27]. In [27] it was explicitly proved for this scenario that the EE across a sphere in flat space is equal to the thermal entropy of the Gibbs state with Unruh temperature T_U. A rerun of the preceding arguments using the regulated horizon in (13), yields the energy per particle

$$\frac{1}{2}\mathcal{E} \sim -\frac{\sqrt{\lambda}}{2\pi} a w_h \tag{23}$$

which can be regarded as the energy of a string in the hyperbolic black hole. The regulated EE as defined by thermodynamics as in (17), now reads

$$S_{\rm EE} = -\frac{\partial \mathcal{E}/2}{\partial a/\beta_h} = -\frac{\sqrt{\lambda}}{2\pi}\beta_h^2 \frac{\partial w_h}{\partial \beta_h} \to \frac{\sqrt{\lambda}}{d-1} \tag{24}$$

with the rightmost result following the removal of the regulator $\mu \to 0$, and in agreement with earlier results [6,29–32]. The difference between (17) and (24) stems from the change in the horizon regulator (21) in (24) through $\partial\mu/\partial w_h \to 2$, in the limit $\mu \to 0$ or $w_h \to 1$. A physical interpretation of this difference will be given below.

2. Topological black hole

Alternatively and in Euclidean signature, we should require that the Wick rotated time (replica) coordinate is an angle with $t = t + 2\pi n$ as we already hinted at in Eq. (20). We can achieve this by replacing the blackening factor $f(w) = -1 + w^2$ by [26,31]

$$f_n(w) = w^2 - 1 - \frac{(w_h^d - w_h^{d-2})}{w^{d-2}},$$
$$w_h = \frac{\sqrt{1 + n^2 d(d-2)} + 1}{nd}, \tag{25}$$

where the horizon is located at $w = w_h$ and $d+1$ is the dimension of the gravity theory.

The regulated metric corresponds to the metric of a charged topological black hole, and the entropy is given by the volume of the horizon region [27]. In fact, replacing the upper integration limit in (13) by the regulated horizon (25), taking the derivative with respect to n and setting $n = 1$ at the end, one gets [6,29–32]

$$S_{\rm EE} = -\frac{\sqrt{\lambda}}{2\pi}(\partial_n(2\pi w_h))_{|n=1} = \frac{\sqrt{\lambda}}{d-1}. \tag{26}$$

This result differs from (17) since an accelerated observer detects quantum fluctuations of the vacuum as they appear to them as thermal fluctuations. In our language these fluctuations are encoded in fluctuations of the horizon which are accounted for by regulating the topological black hole.

3. EE and radiation

If we recall the causal contribution (17), then (26) in $d = 4$ can be represented as

$$S_{\rm EE} = \sqrt{\lambda} - \frac{2}{3}\sqrt{\lambda}, \tag{27}$$

where the first contribution to the entanglement arises from the causal part of the entangling surface (representing the dressing of the charge by virtual gluons), and the second contribution—from the noncausal part of the entangling surface that represents the emitted radiation. In the holographic description, this radiation is hidden behind the world sheet horizon (dual to the Rindler horizon in Minkowski space) as captured by the change in the regulated horizon above. We thus conclude that the emitted radiation reduces the amount of entanglement between the produced particles.

The reduction of the entanglement entropy in the presence of radiation can be expected if we correct the energy per particle (15) for the energy radiated away. Using (11), we find that the energy lost or radiated away from the charged particle is

$$\mathcal{E}_{\rm loss} = \sqrt{\lambda} T_U a \mathcal{T} \sim \sqrt{\lambda} T_U, \tag{28}$$

where we used for the duration of radiation $\mathcal{T}$ the time it takes to reach the world sheet horizon, $\mathcal{T} \sim \frac{1}{a}$.

Our result (27) clarifies the difference between the result in [2], which states that the entanglement entropy of the uniformly accelerated $q\bar{q}$ pair is $S_{\rm EE} = \frac{1}{3}\sqrt{\lambda}$, and the result in [9] which finds $S_{\rm EE} = \sqrt{\lambda}$. The latter takes only the virtual radiation into account (shown in black in 4), while the former also accounts for the real radiation of the moving charged particles (shown in red in 4), which causes energy loss and a decrease in the net entanglement entropy.

B. Walled AdS_5

In order to have a confining background, we introduce a hard wall at $z = z_H$ as in (4). In case of $z_H \geq 1/a$, our calculation reduces to the result of the last section as may be seen from the cartoon in Fig. 3. In the case of $z_H < 1/a$, the surface consists of two parts. The first part corresponds to the minimal surface in the conformal metric, stretching from z_M to z_H is

$$\Delta S_1 = \frac{\sqrt{\lambda}}{2\pi}\int_{-\mathcal{T}/2}^{\mathcal{T}/2} d\tau \int_{z_M}^{z_H} \frac{2dz}{z^2} = \frac{\sqrt{\lambda}}{\pi}\mathcal{T}\left(\frac{1}{z_M} - \frac{1}{z_H}\right). \tag{29}$$

The energy per particle, due to the presence of the hard wall for the first contribution is

$$\frac{1}{2}E_W^{(1)} = \frac{\sqrt{\lambda}}{2\pi}\left(\frac{1}{z_M} - \frac{1}{z_H}\right). \tag{30}$$

It does not contribute to the entanglement, since it does not depend on the Unruh temperature.

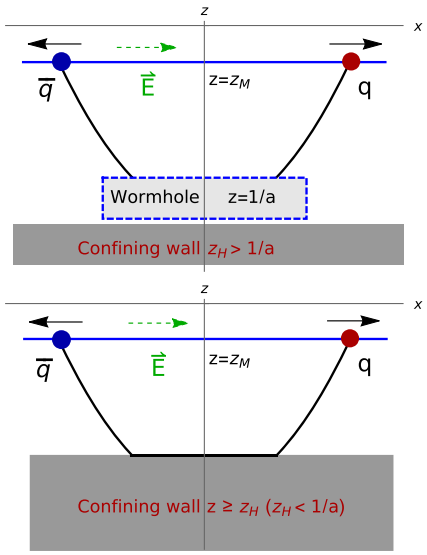

FIG. 3. Top panel: nonconfining case ($z_H > 1/a$). The string world sheet exhibits a nontraversable wormhole with world sheet horizons at $z = 1/a$. The hard wall does not affect the $q\bar{q}$ pair. Lower panel: confining case ($z_H < 1/a$). The world sheet does not have a wormhole which is cut off by the hard wall at $z = z_H < 1/a$.

For the second contribution, we will evaluate the pertinent action. For that, we note that in Euclidean signature, (8) is the spheroidal surface

$$-t^2 + x^2 + z^2 = \frac{1}{a^2} \to t^2 + x^2 + z^2 = \frac{1}{a^2}. \tag{31}$$

The contribution of the hard wall reduces to the area of the disk at the radial position $z = z_H$

$$\Delta S_2 = \frac{\sqrt{\lambda}}{2\pi z_H^2}\pi\left(\frac{1}{a^2} - z_H^2\right) \to \frac{\sqrt{\lambda}}{2(az_H)^2}, \tag{32}$$

with the rightmost term following from the weak field limit. The corresponding free energy is then

$$\beta_U F = \frac{\sqrt{\lambda}\beta_U^2}{8\pi^2 z_H^2}. \tag{33}$$

with $\beta_U = 1/T_U$. The associated entanglement entropy is solely due to (33)

$$S_{\rm EE}^{(2)} = \beta_U^2 \frac{\partial F}{\partial \beta_U} = \frac{\sqrt{\lambda}}{2(az_H)^2}. \tag{34}$$

which can be recast as

$$S_{\rm EE}^{(2)} = \frac{\pi\sigma_T M^2}{E^2}. \tag{35}$$

IV. HOLOGRAPHIC SETUP: STRONG FIELD

The strong electric field analysis of the holographic Schwinger model was initially discussed in the conformal AdS case in [33], and revisited in [5]. The confining and nonconformal case (Sakai-Sugimoto model) was analyzed in [18]. In this section, we follow [5] and review briefly their construction and results in the conformal case, and then proceed to extend them to the confining case using walled AdS.

A. AdS_5

The nonconfining vacuum is unstable against $q\bar{q}$ pair creation for any finite electric field. The creation probability is exponentially suppressed by the action of the tunneling pair through the potential barrier as illustrated in Fig. 1 (bottom). In flat space and at weak coupling, this action follows from the worldline instanton, the cyclotron path traced by a charged quark, in a fixed external electric field, which acts much like a magnetic field in Euclidean signature. The result, is the famed Schwinger suppression factor.

At strong coupling, the holographic construction suggests that the action is that of a world sheet instanton traced by the cyclotron path at the boundary, for infinitely massive quarks. For quarks with finite mass M, the cyclotron path is a Wilson loop on a D3 brane fixed at $z = z_M$ with

$$M = \frac{\sqrt{\lambda}}{2\pi z_M}$$

as measured by the string hanging from D3 to the Poincare horizon. The string world sheet in AdS with Euclidean signature is described by the standard Nambu-Goto action [5]

$$S_{\rm NG} = \frac{\sqrt{\lambda}}{4\pi}\int_0^1 d\tau \int_{\sigma_M}^{\infty} d\sigma \frac{1}{z^2}(\partial X_\mu \bar{\partial} X_\mu + \partial z \bar{\partial} z) + i\oint A, \quad (36)$$

where $(\partial, \bar{\partial}) = (\partial_\sigma \pm i\partial_\tau)$, with the additional Virasoro constraints. The last contribution has support only on the D3 boundary, and captures the effect of the Lorentz force with $F = dA$, on the source quarks,

$$x^M(\tau) = (R\cos(2\pi n\tau), R\sin(2\pi n\tau), 0, 0, z_M) \quad (37)$$

tracing n-times a circular Wilson loop of classical cyclotron radius

$$R \sim \frac{1}{a} = \frac{M}{E}$$

for weak electric fields. For strong fields, the radius shrinks critically to zero (see below). Note that the parameter shift $\tau \to 1/4 - a\tau/2\pi$ in (37) brings (37) into (7).

The variational equations following from (36) and subject to the Virasoro constraints were detailed in [5], with the explicit world sheet solution

$$X^M(\tau,\sigma) = \left(R\cos(2\pi n\tau)\frac{\cosh(2\pi n\sigma_M)}{\cosh(2\pi n\sigma)}, R\sin(2\pi n\tau)\frac{\cosh(2\pi n\sigma_M)}{\cosh(2\pi n\sigma)}, 0, 0, z_M\frac{\tanh(2\pi n\sigma)}{\tanh(2\pi n\sigma_M)}\right), \quad (38)$$

and the condition $\sinh(2\pi n\sigma_M) = z_M/R$. The line-element corresponding to the world sheet instanton (38) is

$$ds_W^2 = \frac{1}{\sinh^2(2\pi n\sigma)}(d\tau^2 + d\sigma^2) \quad (39)$$

Note that (39) develops a singularity at $\sigma \to \infty$,

$$ds_W^2 \to 4e^{-4\pi n\sigma}(-d\tau^2 + d\sigma^2) \quad (40)$$

after the analytical continuation to Minkowski signature $\tau \to i\tau$. This is the conformal line element of a black hole, with Rindler temperature $T_R = 2\pi$ (after rescaling the affine parameters by 2).

Inserting (38) into (36) yields the on-shell action

$$S_{\rm on-shell} = n\sqrt{\lambda}\left(\left(\frac{R^2}{z_M^2}+1\right)^{\frac{1}{2}} - 1\right) - \frac{1}{2}(2\pi n)ER^2. \quad (41)$$

The cyclotron radius R is now fixed by the extremum of (41), which satisfies

$$R^2 + z_M^2 = \frac{1}{a^2} \quad (42)$$

The critical electric field is the electric field for which the cyclotron radius R shrinks to zero, i.e.

$$z_M a_c = z_M\frac{E_c}{M} = 1.$$

In terms of the critical electric field E_c (41), the on-shell action reads [5]

$$S_{\rm on\text{-}shell} = \frac{\sqrt{\lambda}}{2}\left(\sqrt{\frac{E_c}{E}} - \sqrt{\frac{E}{E_c}}\right)^2, \quad (43)$$

This is consistent with Schwinger's result $S \to \frac{\sqrt{\lambda}E_c}{2E}$ in the weak field limit. In the strong field limit, the endpoints of the string on the D3 boundary accelerate substantially, as the cyclotron radius shrinks

$$a_e = \frac{1}{R} = \frac{a}{\sqrt{1-(a/a_c)^2}}. \tag{44}$$

If we recall that the Unruh temperature is $T_U = \frac{a}{2\pi}$ for the pair as it tunnels out of the vacuum, then in Euclidean signature (43) amounts to the free energy

$$\frac{F}{T_U} = \frac{\sqrt{\lambda}}{2}\frac{T_c}{T_U}\left(1-\frac{T_U}{T_c}\right)^2 \tag{45}$$

The entanglement entropy follows from thermodynamics, with

$$S^T_{\rm EE} = \beta_U^2 \frac{\partial F}{\partial \beta_U} = \sqrt{\lambda}\left(1-\frac{T_U}{T_c}\right) \tag{46}$$

and $\beta_U = 1/T_U$. Formula (46) generalizes (17) to the strong field regime. It is the tunneling contribution to the pair creation process. Note that it reduces to the causal contribution (17) (when no real radiation is emitted) in the weak field limit, when $T_U \to 0$.

On the basis of our strong field result (46), and the fact that the result $S_{\rm EE} = \sqrt{\lambda}/3$ holds for any field strength, we can deduce the effect of real radiation on the entanglement entropy in the strong field regime. To reconcile the result for the total entanglement entropy $S_{\rm EE} = \sqrt{\lambda}/3$ with the result (46), we have to assume that the effect of real radiation on the entanglement entropy in the strong field regime is given by

$$S^R_{\rm EE} = -\frac{2}{3}\sqrt{\lambda} + \sqrt{\lambda}\frac{T_U}{T_c}. \tag{47}$$

The strong field calculation described above does not apply for $T_U > T_c$, when the pair production is not exponentially suppressed. This is because the string world sheet has no support for $z < z_M$ (the string calculation breaks down for strictly $R = 0$). Equations (46) plus (47) yield the net result

$$S_{\rm EE} = S^T_{\rm EE} + S^R_{\rm EE} = \sqrt{\lambda}\left(1-\frac{T_U}{T_c}\right) + \sqrt{\lambda}\left(-\frac{2}{3}+\frac{T_U}{T_c}\right) = \frac{\sqrt{\lambda}}{3}, \tag{48}$$

in agreement with (26), even for strong fields. At $T_U = T_c$ the tunneling barrier disappears. For $T_U > T_c$, both the tunneling and the world sheet black hole disappears as the horizon moves below the D3 brane with $\frac{1}{a} < z_M$. The ensuing pair creation process turns "classical," with vanishing entanglement entropy.

The result (48) can be interpreted as follows: The first bracket is the contribution of the virtual gluon interactions to the quantum entropy of a receding pairs, as captured by the tunneling world sheet instanton in bulk (depicted by the green exchanges in Fig. 4 below the blue-dashed line). The second bracket is the contribution to the entanglement entropy from the real emission of gluons by the pair (depicted by the black exchanges with red marks in Fig. 4 above the blue-dashed line).

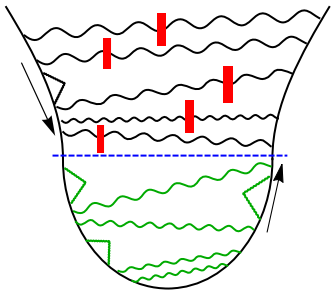

FIG. 4. The trajectories of a produced $q\bar{q}$ pair, with the tunneling part in Euclidean signature (lower half). The dashed blue line marks $t = 0$ where the pair appears in Minkowski space. The virtual radiation is depicted in black and green, and the (real) radiation leading to information loss is marked in red, both in the large N_c planar approximation. The red cut indicates that the exchanged gluon goes on-shell as radiation.

B. Walled AdS_5

In walled AdS_5, the string world sheet terminates on the wall at $z = z_H$, provided that the hard wall occurs prior to the effective horizon $z_M < z_H \le \frac{1}{a}$. Using (31), the contribution of the hard wall is given by the area of the disk at the radial position $z = z_H$

$$\Delta S_2 = \frac{\sqrt{\lambda}}{2\pi z_H^2}\pi\left(\frac{1}{a^2} - z_H^2\right) \tag{49}$$

The corresponding free energy is

$$\beta_U F = \frac{\sqrt{\lambda}}{2}\left(\frac{\beta_U^2}{(2\pi z_H)^2} - 1\right). \tag{50}$$

from which the entanglement entropy reduces to

$$S^{(2)}_{\rm EE} = \beta_U^2 \frac{\partial F}{\partial \beta_U} = \frac{\sqrt{\lambda}}{2}\left(\frac{1}{(az_H)^2} + 1\right) \tag{51}$$

To evaluate the contribution of the side of the string as it reaches the hard wall, we consider the action (36) and the solution (38). The string reaches the hard wall at $z = z_H$. In the world sheet coordinates, the string is parametrized by a continuous function ranging from the starting point of the string at the boundary at $z = z_M$ $(\sigma = \sigma_0)$ to the turning point of the string at $z = z_{\rm max} = \frac{1}{a}$ $(\sigma = \infty)$. On the world sheet this is related to

$$z/z_M = \tanh(2\pi n\sigma)/\tanh(2\pi n\sigma_M)$$

or equivalently

$$2\pi n\sigma = \operatorname{arctanh}\left(\frac{z\tanh(2\pi n\sigma_M)}{z_M}\right).$$

There are two different scenarios. If the cutoff is larger than the turning point of the string $z_H > z_{\max}$, the hard wall does not affect the string, and we find the solution of the last section. If $z_H < z_{\max}$, we cut off part of the string at

$$\sigma_H = \operatorname{arctanh}\left(\frac{z_H\tanh(2\pi n\sigma_M)}{z_M}\right)/(2\pi n).$$

Replacing the upper integration limit in (36) by $\sigma = \sigma_H$, we have

$$\begin{aligned} S_{\text{on-shell}} &= n\sqrt{\lambda}\left(\frac{1}{az_M}-\frac{1}{az_H}\right)-\frac{1}{2}(2\pi n)ER^2 \\ &= \frac{1}{2}\sqrt{\lambda}n\left(\frac{E}{E_c}+\frac{E_c}{E}-\frac{2M}{Ez_H}\right). \end{aligned} \tag{52}$$

Since the cutoff is a hard wall, the radius is still given by (42). For $z_H = z_{\max} = \frac{1}{a}$, the result reduces to (43).

The free energy following from the on-shell action (52) for strong fields, is

$$F = \beta_U^{-1}S_{\text{on-shell}} = \frac{\sqrt{\lambda}n(\pi(\beta_U^2+\beta_c^2)-\beta_U^2\beta_c/z_H)}{2\pi\beta_U^2\beta_c}. \tag{53}$$

The contribution to the entanglement entropy is thus given by

$$S_{\text{EE}}^{(1)} = \beta_U^2\frac{\partial F}{\partial\beta_U} = -n\sqrt{\lambda}\frac{\beta_c}{\beta_U}. \tag{54}$$

Adding the two contributions in (51) and (54), we find for a single winding with $n = 1$

$$\begin{aligned} S_{\text{EE}} &= S_{\text{EE}}^{(1)} + S_{\text{EE}}^{(2)} \\ &= \begin{cases} \sqrt{\lambda}\left(\frac{M^2}{2(Ez_H)^2}+\frac{1}{2}-\frac{E}{E_c}\right) & \text{for: } z_H \le M/E = \frac{1}{a} \\ \frac{1}{3}\sqrt{\lambda} & \text{for: } z_H > M/E = \frac{1}{a} \end{cases}. \end{aligned} \tag{55}$$

with z_H fixed by the string tension in (5), i.e.

$$\frac{\sqrt{\lambda}}{2}\frac{M^2}{(Ez_H)^2} = \frac{\sigma_T}{E}\frac{\pi M^2}{E} \equiv \frac{\sigma_T}{E}\Delta \to \frac{1}{4}\Delta. \tag{56}$$

The rightmost result follows from the estimate for the invariant electric field, as a source for the string tension $E \sim 4\sigma_T$ [24]. Here Δ is the Schwinger tunneling action for pair creation, with probability $e^{-\Delta}$. For a comparison, we note the corresponding Shannon (information) entropy for a single tunneling process

$$S_I = \Delta e^{-\Delta} - (1-e^{-\Delta})\ln(1-e^{-\Delta}) \to \Delta \tag{57}$$

which is comparable to (56) in the weak field limit (rightmost result).

In the limiting case of $z_H = 1/a$, the entanglement entropy in (55) correctly reproduces the entanglement entropy computed in (46). Furthermore, we correctly reproduce the weak field limit in the deconfined case given by (17), as well as the weak field confined case in (34). In Fig. 5 we show the behavior of (55) versus E/E_c. The entanglement is larger in the confining case for weak fields with no radiation loss present, and decreases linearly as the electric field increases following the depletion of the tunneling process. The first order jump occurs when the geometry flips from confining to black hole. The location of the jump varies with M.

General case:

In general for weak electric fields (low Unruh temperature), the entanglement entropy appears to diverge. However, there is a lower bound on the electric field determined by the string tension σ_T

$$\frac{T_{\min}}{T_c} = \frac{E_{\min}}{E_c} > \frac{\sigma_T}{E_c} = \frac{\sqrt{\lambda}}{4\pi^2\alpha' M^2}. \tag{58}$$

To make a contact with QCD phenomenology, we use $\alpha' m_\rho^2 = \frac{1}{2}$ (where m_ρ is the ρ meson mass), and find a light constituent quark mass M, with $M/m_\rho \sim \frac{1}{2}$. If we set $\lambda = g_Y^2 N_c \approx 12$, then the lower bound is

$$\frac{T_{\min}}{T_c} = \frac{E_{\min}}{E_c} > \frac{2\sqrt{\lambda}}{\pi^2} \approx \frac{4\sqrt{3}}{\pi^2} \approx 0.7. \tag{59}$$

In Fig. 5, we display the final result (55) for the entanglement entropy in the confining geometry (blue-solid curve), and the geometry without hard wall (dashed-black curve)

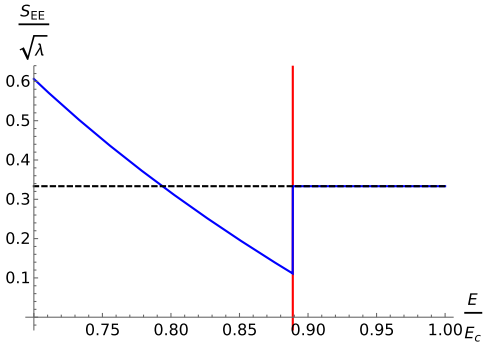

FIG. 5. Entanglement entropy (55) versus E/E_c, in the confining background (blue-solid curve) and the deconfined background (black-dashed curve), for a hard wall at $z_H = 0.89/E_c$ in units of $M = 1$. For $E > 1/z_H$, the entanglement entropies merge. The first order jump reflects on the transition from a confining to a black-hole geometry.

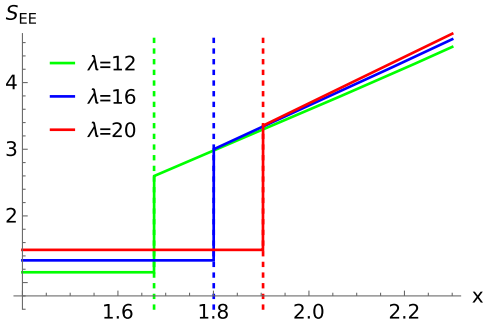

FIG. 6. Entanglement entropy (60) as function of the mass ratio $x = M/m_\rho$ for different 't Hooft coupling λ. The dashed lines indicate $x = \frac{4\lambda^{\frac{1}{4}}}{\pi\sqrt{2}}$.

versus E/E_c in units of $M = 1$. The hard wall is placed at a fixed holographic distance $z_H = 0.89/E_c$. The entanglement entropy is dominated by confinement for $E/E_c < 0.89$, and merges with the entanglement entropy in conformal AdS, as the ER bridge overrides the hard wall in bulk (red line).

Special case:

For the QCD string, the invariant electric field is about $E \sim 4\sigma_T$ [24]. If we also fix the string tension to reproduce the rho meson trajectory $\sigma_T = \frac{1}{2}m_\rho^2$, with a varying mass ratio $x = M/m_\rho$, and a fixed 't Hooft coupling λ, then (55) reduces to

$$S_{\rm EE}(x,\lambda) = \begin{cases} \frac{\pi^2}{16}x^2 + \frac{\sqrt{\lambda}}{2} - \frac{2\lambda}{\pi^2 x^2} & \text{for: } x \geq \frac{4\lambda^{\frac{1}{4}}}{\pi\sqrt{2}} \\ \frac{1}{3}\sqrt{\lambda} & \text{for: } x < \frac{4\lambda^{\frac{1}{4}}}{\pi\sqrt{2}} \end{cases}. \tag{60}$$

In Fig. 6, we illustrate the dependence of the entanglement entropy (60) on the mass ratio x for different values of the 't Hooft coupling λ. For smaller λ, we can reach smaller mass ratios and the deconfinement transition is moving to smaller values of the mass ratio x.

V. ENTROPY IN THE LUND MODEL

A simple but phenomenologically successful description of a hadronization process in QCD, is the Lund model [34], which makes use of the QCD string. The model describes the break-up of the string into hadrons. For instance, as an initial $q\bar{q}$ pair is produced by a hard jet, the connecting string stretches as the pair recedes away from each other. Eventually, several $q\bar{q}$ pair pop up by tunneling, and the stretched string breaks into shorter strings, identified as hadrons (mostly mesons).

A key feature of the multiple break-ups is the so-called area law, at the origin of the probability distribution in the Lund model. The area law is a product of Schwinger tunneling like probabilities, as we have described in the confining case above. Schematically, the normalized probability for the string breaking to n-identical hadrons (say pions) in $1+1$ dimensions, is of the form

$$p_n = (e^A - 1)e^{-nA} \approx (e^{\frac{1}{\bar{n}}} - 1)e^{-\frac{n}{\bar{n}}} \tag{61}$$

Here

$$A \sim \frac{M^2}{\sigma_T} \sim \Delta$$

is a typical fragment area of the string world sheet (in units of the string length squared), with M the light quark constituent mass at the string endpoints. Note that the mean multiplicity $\bar{n}$ and A, are tied by

$$A = -\ln\left(1 - \frac{1}{\bar{n}}\right) \approx \frac{1}{\bar{n}}, \tag{62}$$

which shows that (61) obeys Koba-Nielsen-Olesen (KNO) scaling for large multiplicities

$$\bar{n}p_n \approx e^{-\frac{n}{\bar{n}}} \tag{63}$$

Remarkably, this is a distribution of a thermal oscillator of temperature $T = \bar{n}/\omega$, with ω in units of the string length. The corresponding Shannon (information) entropy is

$$S_{\rm EE} = -\sum_n p_n \ln p_n \approx \ln \bar{n} \tag{64}$$

which we identify as the entanglement entropy of the jet fragmentation. It is a measure of the Schwinger tunneling probability (as weighted by the mean area of the string fragment). Note that the multiple breaking of the string in the Lund model reduces the entanglement entropy compared to the single string breaking (56), from $\frac{1}{4}\Delta$ to $\ln\frac{1}{\Delta}$. The reduction underlines the quantum decoherence caused by the many random breaking on the string world sheet, spanned by the initial receding pair from the jet. It is analogous to the reduction of quantum entanglement by radiation discussed above.

The result (64) is in agreement with the arguments presented in [35,36] for jet fragmentation at large invariant mass. This result was initially noted for pp and ep at small Bjorken x [37,38]. The KNO-based arguments confirm the identification of (64) with the entanglement entropy for QCD, as computed from QCD evolution equations [38]. The fact that (64) is also recovered for the schematic form of the Lund model discussed here, underlines the duality of the partonic and string descriptions of QCD. It also reflects on the Markovian character of both fragmentation processes.

VI. CONCLUSIONS

We have revisited the holographic Schwinger pair creation process in the simplest confining AdS geometry, a slab of AdS_5 with a wall at $z = z_H$. When z_H is removed to infinity, confinement disappears and the pair creation process in curved AdS initially discussed in [5] is recovered for both weak and strong electric fields. As the pair recedes, a holographic string develops with an ER bridge forming in the bulk, encoding geometrically their quantum entanglement [2].

In a dynamical pair creation process, the quantum entanglement entropy is composed of a contribution from the string above the ER bridge, minus the contribution from the string as it enters the ER bridge [6,8]. The latter is dual to the real radiation in the Minkowski space on the boundary. Part of the contribution above the ER bridge can be traced back to the tunneling process. It decreases linearly the stronger the electric field, and vanishes when the field reaches its critical value E_c, for which the potential barrier disappears. The process of pair creation becomes "classical," with no tunneling penalty.

In the presence of confinement, the pair creation process is altered. The creation process occurs only for electric fields in the range $\sigma_T < E < E_c$. For sufficiently weak electric fields in comparison to the string tension σ_T, confinement inhibits the pair creation process, as virtual pairs strongly bind in the vacuum.

For moderately weak fields in the range $\sigma_T < E \ll E_c$, the quantum entanglement is stronger, since the confining scale overrides the ER bridge. The increase in the quantum entanglement of the produced pair is caused by their binding through the string through the hard wall in bulk. For moderately strong electric fields in the range $\sigma_T \ll E < E_c$, the ER bridge overrides the hard wall, with the quantum entanglement reducing to that of the conformal AdS space, and fixed by the causal and noncausal contributions delineated by the ER bridge.

Using the Lund model, as a prototype for string breaking in $1 + 1$ dimensions, we have suggested that the Schwinger tunneling probability is directly related to the entanglement entropy, through the KNO scaling.

The effects of strong coupling on quantum entanglement between the produced particles in time-dependent electric backgrounds is also of great interest. We will report on the results of the corresponding study in a forthcoming publication.

In recent years, the advent of intense lasers and energetic particle beams has led to substantial progress in the study of QED in intense background fields (see [39,40] for reviews). One important nonperturbative phenomenon in this regime is the Schwinger effect. The effects of quantum entanglement in this process have to be explored, and we hope that our work is a step in that direction.

ACKNOWLEDGMENTS

We thank Adrien Florio for useful discussions. This work was supported by the Office of Science, Office of Nuclear Physics, U.S. Department of Energy under Contracts No. DE-FG88ER41450 and No. DE-FG-88ER40388, and by the U.S. Department of Energy, Office of Science, National Quantum Information Science Research Centers, Co-design Center for Quantum Advantage (C2QA) under Contract No. DE-SC0012704 (DK).

[1] Julian S. Schwinger, On gauge invariance and vacuum polarization, Phys. Rev. **82**, 664 (1951).
[2] Kristan Jensen and Andreas Karch, Holographic dual of an Einstein-Podolsky-Rosen pair has a wormhole, Phys. Rev. Lett. **111**, 211602 (2013).
[3] Julian Sonner, Holographic Schwinger effect and the geometry of entanglement, Phys. Rev. Lett. **111**, 211603 (2013).
[4] Bo-Wen Xiao, On the exact solution of the accelerating string in AdS_5 space, Phys. Lett. B **665**, 173 (2008).
[5] Gordon W. Semenoff and Konstantin Zarembo, Holographic Schwinger effect, Phys. Rev. Lett. **107**, 171601 (2011).
[6] Aitor Lewkowycz and Juan Maldacena, Exact results for the entanglement entropy and the energy radiated by a quark, J. High Energy Phys. 05 (**2014**) 025.
[7] Mariano Chernicoff, Alberto Güijosa, and Juan F. Pedraza, Holographic EPR pairs, wormholes and radiation, J. High Energy Phys. 10 (2013) 211.
[8] Kristan Jensen, Andreas Karch, and Brandon Robinson, Holographic dual of a Hawking pair has a wormhole, Phys. Rev. D **90**, 064019 (2014).
[9] Veronika E. Hubeny and Gordon W. Semenoff, Holographic accelerated heavy quark-anti-quark pair, arXiv:1410.1172.
[10] Mahdis Ghodrati, Schwinger effect and entanglement entropy in confining geometries, Phys. Rev. D **92**, 065015 (2015).
[11] Gordon W. Semenoff, Lectures on the holographic duality of gauge fields and strings, 10.1093/oso/9780198828150.003.0003 (2018).
[12] Juan Maldacena and Leonard Susskind, Cool horizons for entangled black holes, Fortschr. Phys. **61**, 781 (2013).

[13] Jan de Boer, Viktor Jahnke, Keun-Young Kim, and Juan F. Pedraza, Worldsheet traversable wormholes, J. High Energy Phys. 05 (2023) 141.
[14] Dmitri Kharzeev and Kirill Tuchin, From color glass condensate to quark gluon plasma through the event horizon, Nucl. Phys. **A753**, 316 (2005).
[15] Berndt Müller and Andreas Schäfer, Quark-hadron transition and entanglement, arXiv:2211.16265.
[16] Adrien Florio and Dmitri E. Kharzeev, Gibbs entropy from entanglement in electric quenches, Phys. Rev. D **104**, 056021 (2021).
[17] Adrien Florio, David Frenklakh, Kazuki Ikeda, Dmitri Kharzeev, Vladimir Korepin, Shuzhe Shi, and Kwangmin Yu, Real-time nonperturbative dynamics of jet production: Quantum entanglement and vacuum modification, Phys. Rev. Lett. **131**, 021902 (2023).
[18] Keun-Young Kim, Sang-Jin Sin, and Ismail Zahed, Dense and hot holographic QCD: Finite baryonic E field, J. High Energy Phys. 07 (2008) 096.
[19] Yizhuang Liu and Ismail Zahed, Entanglement in Regge scattering using the AdS/CFT correspondence, Phys. Rev. D **100**, 046005 (2019).
[20] G. E. Volovik, Particle creation: Schwinger + Unruh + Hawking, JETP Lett. **116**, 595 (2022).
[21] Andrei Mikhailov, Nonlinear waves in AdS/CFT correspondence, arXiv:hep-th/0305196.
[22] Juan Martin Maldacena, Wilson loops in large N field theories, Phys. Rev. Lett. **80**, 4859 (1998).
[23] Joshua Erlich, Emanuel Katz, Dam T. Son, and Mikhail A. Stephanov, QCD and a holographic model of hadrons, Phys. Rev. Lett. **95**, 261602 (2005).
[24] A. Casher, H. Neuberger, and S. Nussinov, Chromoelectric flux tube model of particle production, Phys. Rev. D **20**, 179 (1979).
[25] J. Antonio Garcia, Alberto Güijosa, and Eric J. Pulido, No line on the horizon: On uniform acceleration and gluonic fields at strong coupling, J. High Energy Phys. 01 (2013) 096.
[26] Roberto Emparan, AdS/CFT duals of topological black holes and the entropy of zero energy states, J. High Energy Phys. 06 (1999) 036.
[27] Horacio Casini, Marina Huerta, and Robert C. Myers, Towards a derivation of holographic entanglement entropy, J. High Energy Phys. 05 (2011) 036.
[28] Veronika E. Hubeny and Gordon W. Semenoff, String worldsheet for accelerating quark, J. High Energy Phys. 10 (2015) 071.
[29] Han-Chih Chang and Andreas Karch, Entanglement entropy for probe branes, J. High Energy Phys. 01 (2014) 180.
[30] Andreas Karch and Christoph F. Uhlemann, Generalized gravitational entropy of probe branes: Flavor entanglement holographically, J. High Energy Phys. 05 (2014) 017.
[31] Adam Chalabi, S. Prem Kumar, Andy O'Bannon, Anton Pribytok, Ronnie Rodgers, and Jacopo Sisti, Holographic entanglement entropy of the Coulomb branch, J. High Energy Phys. 04 (2021) 153.
[32] Xin-Xiang Ju, Wen-Bin Pan, Ya-Wen Sun, and Yuan-Tai Wang, Entanglement entropy of generalized Rindler wedge, arXiv:2302.03340.
[33] A. S. Gorsky, K. A. Saraikin, and K. G. Selivanov, Schwinger type processes via branes and their gravity duals, Nucl. Phys. **B628**, 270 (2002).
[34] Bo Andersson, G. Gustafson, G. Ingelman, and T. Sjostrand, Parton fragmentation and string dynamics, Phys. Rep. **97**, 31 (1983).
[35] Yizhuang Liu, Maciej A. Nowak, and Ismail Zahed, Mueller's dipole wave function in QCD: Emergent KNO scaling in the double logarithm limit, Phys. Rev. D **108**, 034017 (2023).
[36] Yizhuang Liu, Maciej A. Nowak, and Ismail Zahed, Universality of Koba-Nielsen-Olesen scaling in QCD at high energy and entanglement, arXiv:2302.01380.
[37] Alexander Stoffers and Ismail Zahed, Holographic Pomeron and entropy, Phys. Rev. D **88**, 025038 (2013).
[38] Dmitri E. Kharzeev and Eugene M. Levin, Deep inelastic scattering as a probe of entanglement, Phys. Rev. D **95**, 114008 (2017).
[39] Gerald V. Dunne, Heisenberg-Euler effective Lagrangians: Basics and extensions, in *From Fields to Strings: Circumnavigating Theoretical Physics. Ian Kogan Memorial Collection (3 Volume Set)*, edited by M. Shifman, A. Vainshtein, and J. Wheater (World Scientific, 2004), pp. 445–522.
[40] A. Fedotov, A. Ilderton, F. Karbstein, B. King, D. Seipt, H. Taya, and G. Torgrimsson, Advances in QED with intense background fields, Phys. Rep. **1010**, 1 (2023).